PAPER

Nacre-inspired layered composite gels with broad tunable mechanical strength and structural color for stress visualization†

Yunpeng Wang, Xinyu Kan, Yaru Liu, [ID] Jie Ju [ID] * and Xi Yao [ID] *

The brick-and-mortar architecture of nacre shells brings radiant structural colors, high toughness, and strength, inspiring numerous designs for structural and optical materials. However, constructing structural color is not always easy, especially among soft materials where aligning components against random and dynamically active environments is generally difficult. Here, we propose a composite organohydrogel capable of visualizing multiple levels of stress, featuring broad tunable mechanical properties, dynamic mechanochromism, deep low working temperatures, and anti-drying attributes. In the composite gels, the intercalation between α-zirconium phosphate (α-ZrP) nanoplates and poly-(diacetone acrylamide-*co*-acrylamide) is induced by shear-orientation-assisted self-assembly followed by solvent replacement. The highly tailorable (from ~780 nm to ~445 nm) range of colors was achieved by regulating the concentration of α-ZrP and glycerol inside the matrix. With the help from glycerol, the composite gels exhibited long-term stability (7 d) in the arid condition and remarkable low-temperature tolerance (−80 °C). The extraordinary mechanical property (compressive strength up to 119 MPa) of composite gels is achieved by the assembled α-ZrP plates with a small aspect ratio, high negative charge repulsion, and abundant hydrogen bonding sites. As a result, the mechanochromic sensor based on the composite gel enjoys a wide range of stress detection (0–1862 KPa). This study provides a new strategy for constructing high strength structural-colored gels, opening up opportunities for sensitive yet strong mechanochromic sensors in extreme environments.

Key Laboratory for Special Functional Materials of Ministry of Education, School of Materials and Engineering, Henan University, Kaifeng 475000, China.
E-mail: yaoxi@henu.edu.cn, jujie@henu.edu.cn

†Electronic supplementary information (ESI) available: Specific component of solution A containing polymeric monomers (Table S1). Digital images of α-ZrP suspension under gravity (Fig. S1). (a) SEM image and (b) lateral size distribution of the original α-ZrP nanoplates (Fig. S2). Polarizing light microscopic images of photonic LC suspensions (Fig. S3). SAXS profiles of the α-ZrP suspensions (Fig. S4). Reflection spectra of composite hydrogels prepared based on different mass fractions of α-ZrP suspensions (Fig. S5). Reflection spectra of composite gels after solvent replacement and heating treatment (Fig. S6). Weight changes of composite gels during heating treatment (Fig. S7). Weight change of the composite gels with time at 35% RH (Fig. S8). Weight of a composite gel sample at different RH (Fig. S9). DSC spectra of composite gels (Fig. S10). Tensile stress–strain curves of composite gels prepared with different crosslinker contents (Fig. S11). Solvent content and reflection wavelength of composite gels prepared with different crosslinker contents (Fig. S12). Specific component of solution A containing AAM : DAAM monomer ratio (Table S2). (a) Tensile stress–strain curves of composite gels prepared with different AAM : DAAM monomer ratio in Table S2. (b) Solvent content of corresponding samples before and after heating treatment (Fig. S13). Tensile stress–strain curves of pure PDAAM-*co*-PAAM gels matrix prepared with different crosslinker contents (Fig. S14). Reflection spectra evolution of composite gels with different crosslinker contents under different compression stress (Fig. S15). Digital images showing applied compressive stresses and structural color changes (Fig. S16). See DOI: https://doi.org/10.1039/d3nr01362f

Introduction

Structural colors, deriving from long/short-range ordered photonic nanostructures, are found on diverse organisms, such as chameleons,[1] nacre shells,[2] cephalopods,[3] *etc*. Mimicking these natural nanostructures, a large number of artificial-structural-colored materials have been developed based on the assembly of colloidal microspheres, cellulose, block copolymers, or two-dimensional (2D) nanosheets.[4–8] Among these, structural color switching in gels can be mechanically triggered by inducing changes in lattice space or diffraction angles. Structural-colored gels can provide visual feedbacks for changes and distribution of strain/stress, which make them promising in fields of mechanochromic sensor, health monitor, anti-counterfeit labels, display, *etc*.[9–14] Most structural-colored gels are highly mechanically sensitive due to their low moduli. They are good at quantitative analysis and spatial mapping for small stress (<100 KPa).[10,15–18] However, practical applications usually call for structural-colored gels with broader responses as well as load-bearing stability that typically range from 100 KPa–100 MPa.

Nacre shells not only show fascinating structural colors but also extraordinary mechanical stability.[19,20] These two characteristics originate from the brick-and-mortar (BM) photonic architecture and intercalation between a high fraction of hard $CaCO_3$ nanoplates and low fraction of soft biopolymers (Fig. 1). Inspired by such a structure, researchers used inorganic 2D nanomaterials and organic polymer to fabricate nacre-like structural nanocomposites with light-weight and high strength features.[21–23] We can also utilize such structures in colored gels with better mechanical properties. In fact, some particular monolayer nanosheets can self-assemble into liquid crystals (LCs) with swollen lamellar structures balanced by entropic interactions and electrostatic repulsion. The so-named photonic LCs exhibit structural colors.[24–29] However, in contrast to the high fraction of $CaCO_3$ nanoplates in nacre shells, the fraction of nanosheets in photonic LCs is rather low.[30] Such a low fraction makes the as-prepared structural-colored gels weak and fragile.[31] Therefore, we are now facing conflicting requirements for optical responsiveness and load-bearing stability.

In this paper, by fully mimicking nacre's BM architecture, we present a novel class of layered composite gels with nacre-like structural colors and broad tunable mechanical properties. As shown in Fig. 1, the gels consist of α-ZrP nanoplates (as "bricks") bonded by poly-(diacetone acrylamide-co-acryl-amide) (PDAAM-co-PAAM) (as the "mortar"). The α-ZrP is inorganic layered nanoplates with a small aspect ratio (lateral dimension/thickness) and negative surface charge. Thus, it can self-assemble into nematic photonic LCs rather than agglomerate based on Onsager's excluded volume effects at high concentrations.[32] By virtue of this characteristic, the alternating hard/soft composite gels are realized by self-assembly of nanoplates into roughly ordered structures in the suspension mixed with polymer precursors, followed by immobilization in a soft gel matrix with the assistance of shear orientation and photopolymerization. In order to prevent structural color degradation or disappearance due to dehydration in ambient air, solvent displacement methods and heating treatments were implemented to improve optical stability. As a result, the as-prepared composite gels have remarkable anti-drying/anti-freezing properties arising from hydrogen bonding formed by glycerol (Gly) and water, as well as dynamically reversible mechanochromic behavior. Importantly, α-ZrP nanoplates contain a high density of hydroxyl groups, which can easily form dense hydrogen bonding with polymer chain segments to provide stable interfacial bonding, so they substantially improve the mechanical strength of the composite gels. In addition, the mechanical strength of composite gels is broadly modulated by adjusting the crosslinking concentration. On this basis, we successfully established the quanti-
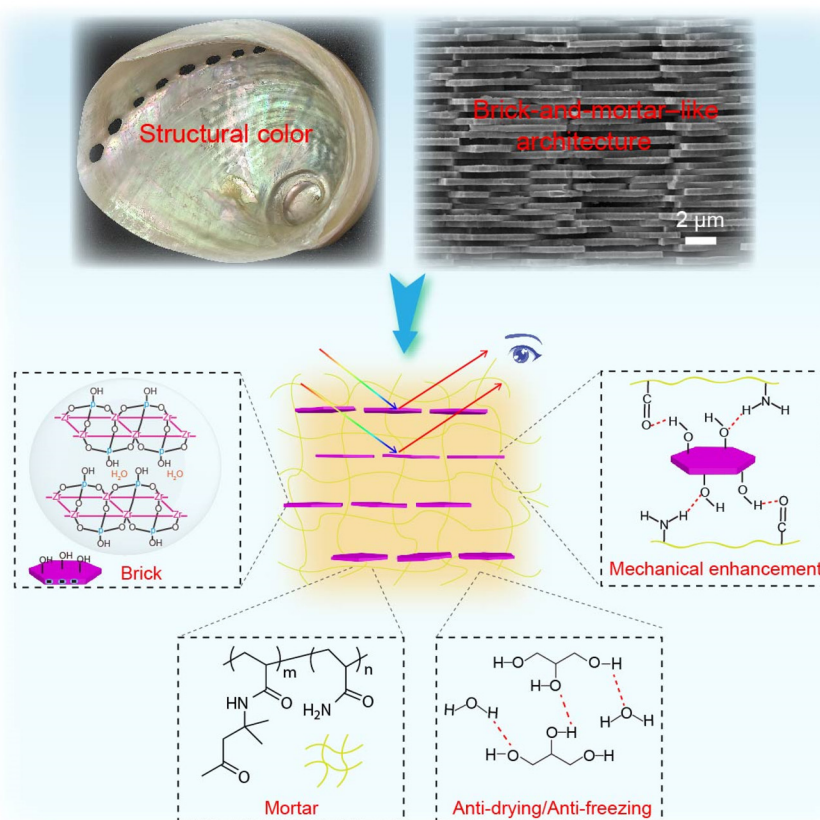

Fig. 1 Concept diagram of layered composite gels inspired by the nacre layer of shell.

tative relationships between stress and structural color in a large window, turning to visualize different levels of stress.

Experimental

Materials

Original α-ZrP was purchased from Sunshine Factory Co., Ltd. Diacetone acrylamide (DAAM), acrylamide (AAM), N,N-methylene bisacrylamide (MBAA), Gly, and 2-hydroxy-2-methyl-propiophenone (1173) were purchased from Aladdin Chemical Co. Carbon black (30 nm) was purchased from Adamas-beta®.

Gravity fractionation of α-ZrP

Firstly, α-ZrP (10 g) was dispersed in deionized water (40 mL) with vortex shaking for 1 min, followed by sonication for 1 min to disperse α-ZrP evenly in the water. Subsequently, the suspension was transferred to a 50 mL centrifuge tube and allowed to stand for 20 h. Then, 20%–80% of the fractions were collected by centrifugation (7000 rpm, 2 min). Finally, the obtained α-ZrP was dried in an oven at 65 °C for 24 h.

Preparation of photonic LC suspensions containing polymeric monomers

Firstly, polymerizable monomers DAAM, AAM, crosslinker MBAA, and photoinitiator 1173 were added to deionized water and dissolved by ultrasonication for 10 min to obtain solution A (see Table S1† for the specific components). Subsequently, the fractionated α-ZrP was dispersed in a solution with vortex shaking for 1 min, followed by sonication for 1 min to obtain photonic LC suspensions with different α-ZrP mass fractions (45 wt%–60 wt%). To brighten the structural color of the LC, 5 μL carbon black aqueous solution (1 wt%) was added to 1 g photonic LC suspensions. It should be noted that the crosslinker in solution A is 16 mg when it is not specified in this work.

Preparation of layered α-ZrP composite gels

Firstly, a polymerization reaction cell was prepared by sandwiching double-sided adhesive (0.5 mm thick) between two pieces of parallel transparent glass. Secondly, the photonic LC suspensions were injected into the reaction cell and then cured by UV (365 nm, 18 W) for 10 min, and the layered α-ZrP composite hydrogels were obtained. Thirdly, the displacement solvents were obtained by mixing Gly (20 wt%–50 wt%) with water. Fourthly, the as-synthesized hydrogels were immersed in a Gly–water mixture for 24 h for solvent replacement, and the swollen organohydrogels were obtained subsequently. Finally, the swollen organohydrogels were placed in an oven at 65 °C for 90 min to volatilize the extremely unstable free water inside gel networks so as to obtain the required layered α-ZrP composite gels.

Preparation of PDAAM-co-PAAM organohydrogel matrix

Firstly, solution A was injected into the reaction cell and then cured by UV for 5 min. Secondly, the obtained PDAAM-co-PAAM hydrogel matrix was immersed in the Gly–water mixture for 24 h for solvent replacement. Then, the swollen organohydrogels were placed in an oven at 65 °C for 90 min so as to obtain the required PDAAM-co-PAAM organohydrogel matrix.

Characterizations

SEM images were taken by scanning electron microscope (JSM-7900F). AFM image was taken with an atomic force microscope (Dimension Icon). Zeta potential of α-ZrP was measured by zeta potential analyser (ZS90). Polarizing images were taken through an optical microscope (Axioscope5). The mechanical compression/tension tests were performed by an electronic universal material testing machine (INSTRON5965, Instron Corporation), where rates of compression and tension were 1 mm min⁻¹ and 20 mm min⁻¹, respectively. The normal-incidence reflection spectra were obtained by using a fibre-optic spectrometer (USB2000, Ocean Optics (SHANGHAI) Co., Ltd). DSC spectra were measured by differential scanning calorimetry on DSC250 TA. Low temperature environment (−80 °C) is provided by the medical cryopreservation box (MDF-86V50). The structural color patterns were obtained when the samples were pressed by the convex seals, where the presented pressure values were estimated from the variation relationship between the reflection wavelength and compressive stress.

Results and discussion

Preparation of photonic LC suspensions with adjustable structural color

The flowchart of preparing the photonic LC suspensions is schematically depicted in Fig. 2a. In detail, we first added polymerizable monomer DAAM, AAM, and crosslinker MBAA to deionized water to obtain solution A (Table S1†), which was intended for subsequent construction of the soft gel matrix. Then, the fractionated α-ZrP was uniformly dispersed in solution A after vortex oscillation and ultrasound and self-assembled to form swollen nematic LC driven by Onsager's excluded volume effects and electrostatic repulsion between charged nanoplates (63.8 ± 0.4 mV). This swollen nematic LC would undergo Bragg diffraction with natural light, thus reflecting broad-spectrum wavelength to produce structural color. In addition, trace amounts of carbon black were added to the suspension to absorb stray light to enhance the structural color.[33] In order to enable the formation of photonic LCs in the aqueous phase, the original α-ZrP nanoplates with polydisperse morphology need to be fractionated by gravitational sedimentation, reducing its polydispersity (see Experimental section, Fig. S1†).[32] As shown in Fig. 2b, c and S2,† after the fractionation treatment, the average lateral size of α-ZrP shifts from 1.64 ± 0.58 μm to 1.55 ± 0.35 μm, and the fractionated α-ZrP has a rather narrow normal distribution than original one.

We expect α-ZrP to form a nematic phase at high concentrations because high fractional reinforcement can significantly improve the mechanical strength of composite gels.
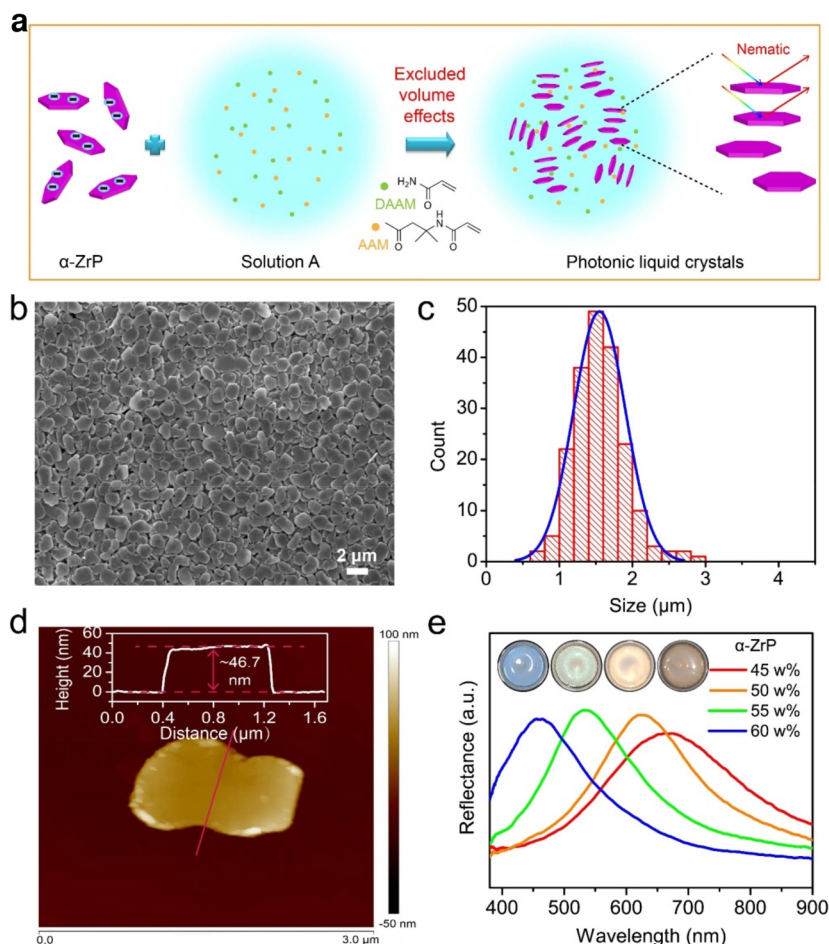
Fig. 2 (a) SEM image and (b) lateral size distribution of the fractionated α-ZrP nanoplates. (c) Schematic illustration showing preparation process of the photonic LC suspensions. (d) AFM image of α-ZrP nanoplates, the inset is height profile. (e) Reflection spectra of the suspensions prepared with different mass fractions of α-ZrP, the insets show the corresponding structural color variation.

According to Onsager's theory, the critical concentration of nematic phase (Φ_{LC}, volume fraction) in a nanoplate suspension system conforms to the following equation:[30]

$$\Phi_{LC} = 4.5 \left(\frac{4L}{\pi D} \right)$$

where L represents the thickness, and D represents the lateral dimension of the nanoplates. In consequence, the system with a smaller aspect ratio (D/L) tends to convert from isotropic to nematic phase at higher fractions. In this work, the thickness of α-ZrP measured by AFM image is ~46.7 nm (Fig. 2d). We assumed an average lateral dimension of 1.55 μm for α-ZrP, and the aspect ratio was estimated to be 33.2, subsequently. Thus, a theoretical Φ_{LC} should be 17.3% by calculation. For simplicity, we deduced a critical mass fraction of 45.1 wt% based on the density of α-ZrP (3.3 g mL^{-1}) and solution A (0.84 g mL^{-1}, experimentally measured). Compared to photonic LC systems formed by monolayer nanosheets at low concentrations (0.09%–1.34%, volume fraction),[24,29] high fraction α-ZrP LC clearly caters more to our needs to enhance the mechanical strength of photonic gels.

In fact, when the mass fraction of α-ZrP was above 45 wt%, we also successfully obtained the photonic LC suspensions with structural color (Fig. 2e). This is consistent with the results predicted by the above theory. At the same time, we also observed the obvious birefringence of the suspension under the polarized light microscope (Fig. S3†), indicating that the LC structure has been formed. We further demonstrated that α-ZrP formed a nematic phase by small-angle X-ray scattering (SAXS) since no typical scattering peaks at the scattering vector (q) ratio of 1 : 2 : 3 were found (Fig. S4†). By stepwise increasing the proportion of α-ZrP (from 45 wt% to 60 wt%), the structural color blue-shifted from red (~665 nm) to blue (~460 nm) accordingly. This blue-shift behaviour can be explained by the following Bragg equation:

$$\lambda = 2nd \sin \theta$$

where λ, n, d, θ represent the reflection wavelength, effective refractive index, average interlayer spacing between adjacent nanoplates, and incidence angle,[13] respectively. The increasing α-ZrP led to a decrease in interlayer spacing, thereby resulting in a blue shift in the reflection wavelength of the suspension.

Layered composite gels with brick-and-mortar-like architecture and mechanochromism

Fig. 3a shows a flowchart of constructing layered composite gels by *in situ* immobilizing hard photonic LCs in soft polymers. Since photonic LC microdomains are usually randomly oriented in suspension, we need to use a shear-field-assisted strategy to orient them.[34,35] Specifically, we injected the above suspension into a reaction cell consisting of two parallel glasses, and α-ZrP nanoplates would be induced to align in parallel orientation by shear forces generated at the liquid-glass interface. The layered composite hydrogels were then constructed by UV curing. A series of composite hydrogels, prepared based on different mass fractions of α-ZrP suspensions, exhibited broad reflection spectra and corresponding nacre-like structural colors, indicating the nematic structure was successfully immobilized in the PDAAM-*co*-PAAM hydrogel matrix (Fig. S5†). To prevent the structural color from blue-shifting or disappearing in ambient air due to matrix dehydration, the as-synthesized composite hydrogels were immersed in the Gly–water mixture for solvent replacement and were transformed into swelling composite organohydrogels. Finally, the extremely unstable free water in the polymer network was volatilized by heat treatment at 65 °C, and thus the desired layered composite gels with anti-drying ability were prepared.

By observing the cross-section of gel with a polarized optical microscope, anisotropic interference color caused by birefringence can be seen (Fig. 3b), proving that the gel has a macroscopically anisotropic structure.[21,31] Meanwhile, it can be seen from the surface and cross-sectional SEM images that the nanoplates are indeed stacked parallel to the gel surface (Fig. 3c and d), further demonstrating that the nanoplates are directionally aligned to form an anisotropic structure under shear-induced action, similar to nacre's BM architecture. The structural color of the composite gels is highly tailorable by varying the concentration of α-ZrP and Gly, respectively. As displayed in Fig. 3e, with a fixed Gly mass fraction of 50 wt% in the replacement solvent, the reflection wavelength of the composite gels was regulated from ~775 nm to ~600 nm by increasing α-ZrP concentration from 45 wt% to 60 wt%, analogous to the optical change of the suspensions. Along with the regulation of Gly from 20 wt% to 50 wt%, a series of composite
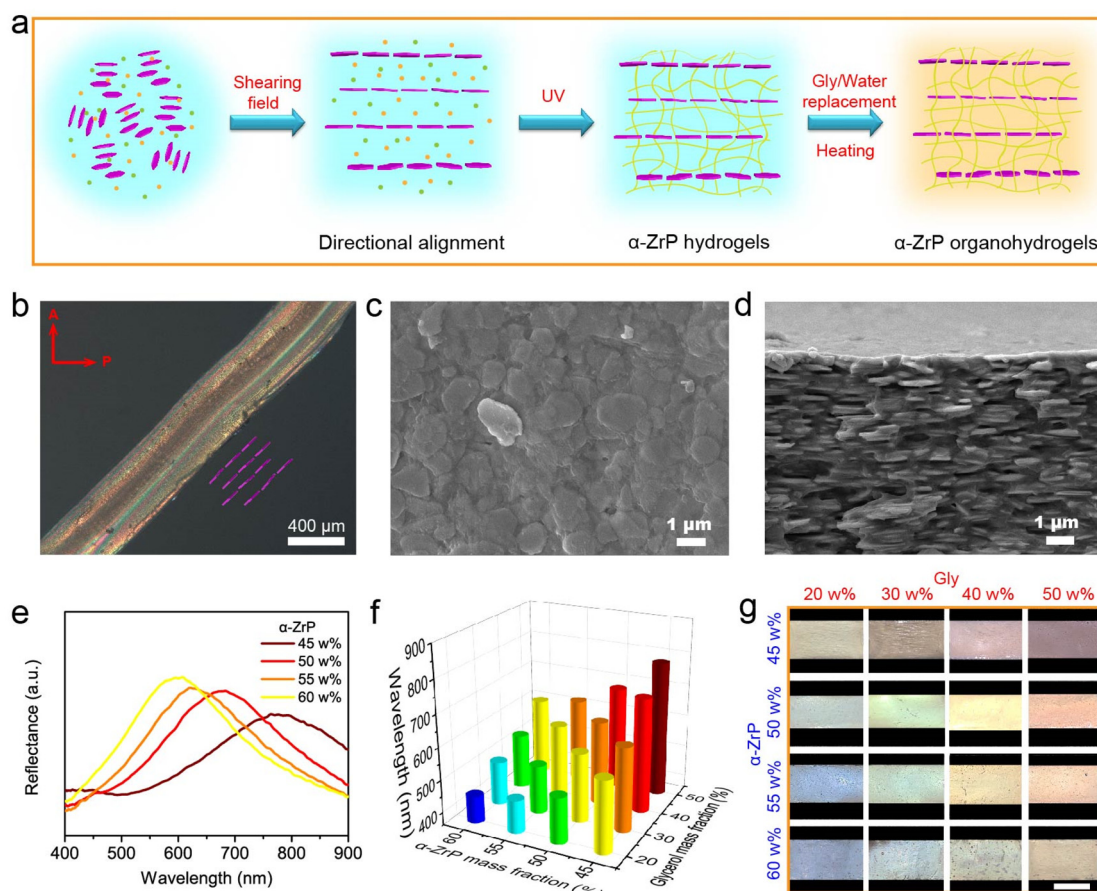

Fig. 3 (a) Schematic illustration showing the preparation process of layered composite gels. (b) Cross-sectional polarizing light microscopic image of the composite gels, interpolation diagram reflects the anisotropic arrangement of α-ZrP nanoplates inside gels. (c) Surface and (d) cross-sectional SEM images of the sample. (e) Reflection spectra of composite gels after 50 wt% Gly replacement and 65 °C heating treatment. (f) Reflection wavelength and (g) corresponding structural colors of composite gels prepared with varying α-ZrP and Gly mass fractions, scale bar is 1 cm.

gels with different reflection wavelengths and structural colors were developed with four α-ZrP concentrations, as shown in Fig. 3f, g and S6.† It can be found that the Gly proportion decreases for the same α-ZrP concentration, the reflection wavelength blue-shifts, and the gels exhibit corresponding structural color switching. This blue-shift phenomenon is caused by the different degrees of water volatilization in the polymer network. Specifically, with the decrease in Gly content, the higher the water content of the swelling organohydrogels, the greater the mass loss after heating treatment (Fig. S7†), and the interlayer spacing between the nanoplates tends to be smaller. Thus, with synergistic regulation of α-ZrP and Gly concentrations, structural colors across the wide visible spectrum range (from ~780 nm to ~445 nm) can be obtained. In the subsequent work, the red composite gels were selected to investigate the mechanochromic properties, which were polymerized by 50 wt% α-ZrP suspension and replaced by 50 wt% Gly solvent.

We demonstrated the optical stability of the composite gels after Gly–water displacement and heating treatment in ambient air. Since the unstable free water in the polymer network has been volatilized during the heating treatment process, the weight of the sample did not change during the observation period of 7 days, even under the arid condition of 35% relative humidity (RH) (Fig. S8†). This indicates that the as-prepared composite gels exhibit significant long-term solvent retention. As such, its reflection wavelength also does not change (Fig. 4a), which is very favorable for structural-colored gels to exhibit mechanochromism in ambient air. Considering the strong hygroscopicity of Gly, we also tested

the influence of typical humidity in the air on the structural color of composite gels. As shown in Fig. 4b, with the increase in humidity from 35% RH to 75% RH, although the reflection wavelength of sample undergoes a slight red-shift from ~645 nm to ~710 nm, this red-shift does not lead to the disappearance of structural color. The red-shift phenomenon is caused by the increase in the nanoplate interlayer spacing due to the trapping of airborne water *via* Gly in the matrix (Fig. S9†). Additionally, our composite gels also demonstrate excellent freezing tolerance at extremely low temperatures. As shown in Fig. 4c, the reflection spectrum of the sample, placed at −80 °C for 48 h, is almost consistent with its counterpart at room temperature. What is more, we also did not observe the peak representing the freezing point in a dynamic scanning calorimetry (DSC) spectrum (from 20 °C to −80 °C), and the sample could still be bent at −80 °C (Fig. S10†), which could be ascribed to the formation of hydrogen bonds between Gly and water molecules to inhibit the formation of ice nucleation.[36,37] This result reflects that the composite gels have an extremely low freezing point and low-temperature tolerance.

Based on the remarkable resistance to drying and freezing, our layered composite gels present great potential for applications in mechano-colorimetric-sensors. Fig. 4d shows the continuous evolution of reflection spectra when compressive strain is applied to the gels. Along with the strain increasing from 0% to 35%, the reflection wavelength synchronously blue-shifts from ~648 nm to ~540 nm. The stepwise changes from red to green of the corresponding structural colors can also be visually observed in Fig. 4e. This strain-induced color
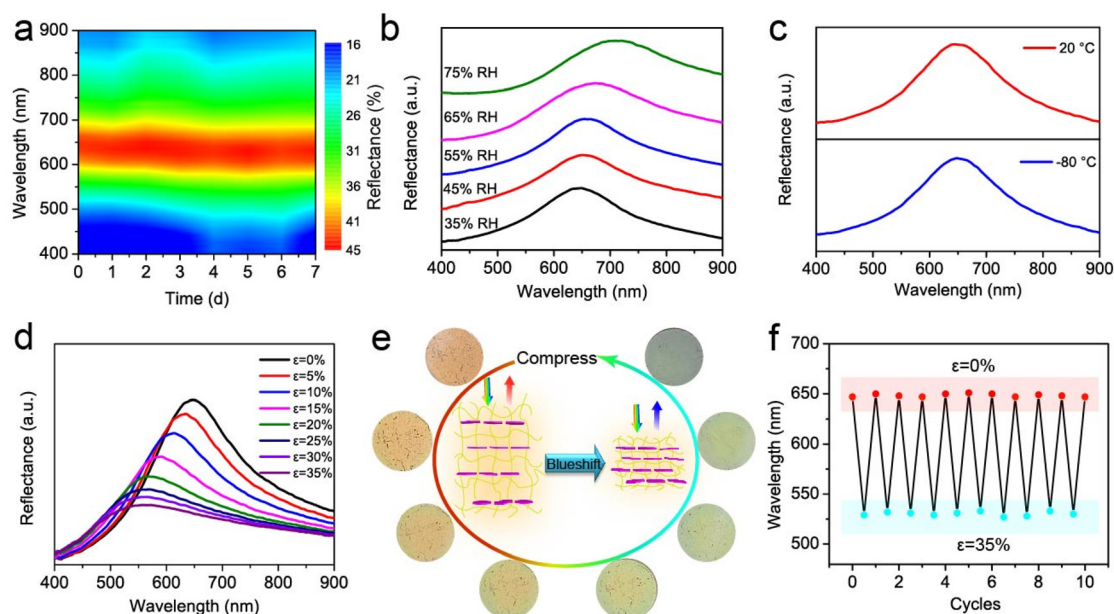

Fig. 4 (a) Color filled contour maps showing reflection spectra change of the layered composite gels with time at 35% RH. (b) Reflection spectra of the sample at different relative humidity. (c) Reflection spectra of the sample at 20/−80 °C for 48 h. (d) Reflection spectra evolution of the sample under different compression strain. (e) Compression-induced stepwise color variation of the corresponding sample. Inset shows blue-shift mechanism under compression. (f) Reversible changes in reflection wavelength at 10 loading/unloading of the compressive strain.

change stems from the deformation of gels forcing the soft polymer to shrink along the direction perpendicular to the nanoplates, thus shortening the interlayer spacing between adjacent nanoplates. Importantly, with repeated loading/uploading of the compressive strain, the structural color change is dynamically reversible, and the reflection wavelength position can be fully recovered after strain release, as shown in Fig. 4f. The above results demonstrate that the as-prepared composite gels have excellent mechanochromic capability.

Adjustable mechanical strength and stress visualization

Layered composite gels exhibit high-strength mechanical properties and broad tunability. As shown in Fig. 5a and S11,† we prepared a series of composite gels with distinct mechanical strengths by adjusting the content of crosslinker MBAA in solution A (see TableS1†). Typically, with the increase in crosslinker content from 2 mg to 64 mg, the compressive strength of the gels leaps from ~3.66 MPa to ~119 MPa under 80% compression; the tensile fracture strength also increases from ~0.23 MPa to ~2.59 MPa, proving that the mechanical properties can be modulated over a large window. This apparent difference is mainly caused by the synergistic effect of two factors: on the one hand, the crosslinking density of the gel matrix gradually increases with the MBAA concentration; on the other hand, the high crosslinking density further leads to a gradual reduction of the displacement solvent content inside the gel matrix (Fig. S12†), which in turn causes an increase in the polymer network density.[38] Notably, all composite gels did

not break at 80% compressive strain, and the compressive strength was much higher than the tensile strength. This is due to the highly negatively charged α-ZrP nanoplates arranged in parallel, and the strong electrostatic repulsion generated between the nanoplates during compression leads to significant compressive strain-hardening.[31] Afterward, we also explored the influence of different AAM/DAAM ratios on the mechanical properties of the composite gels (Table S2 and Fig. S13a†). The mechanical properties were gradually enhanced with the increase in the DAAM monomer ratio. This is because PDAAM is a typical hydrophobic polymer, and its increasing proportion leads to a decrease in the hydrophilic solvent content within the matrix (Fig. S13b†),[39] as well as an increase in the polymer network density.

Furthermore, by comparing the mechanical properties of the composite gels and the pure PDAAM-*co*-PAAM gel matrix, we also confirmed the validity of the nacre-mimetic BM architecture. As shown in Fig. 5a, b and S11, S14,† respectively, the compressive strength and tensile strength of composite gels are significantly higher than that of the pure gel matrix. For example, the compressive strength (~119 MPa) of the composite gels, prepared with 64 mg crosslinker in solution A, is about 25.4 times that of the pure gels (~4.66 MPa) under 80% compressive strain; also, the tensile fracture strength (~2.59 MPa) is about 18.8 times that of pure gels (~0.13 MPa). This superior reinforcement is due to the high fraction α-ZrP, whose numerous surface hydroxyl groups can form dense hydrogen bonding with amide groups on the polymer chain,
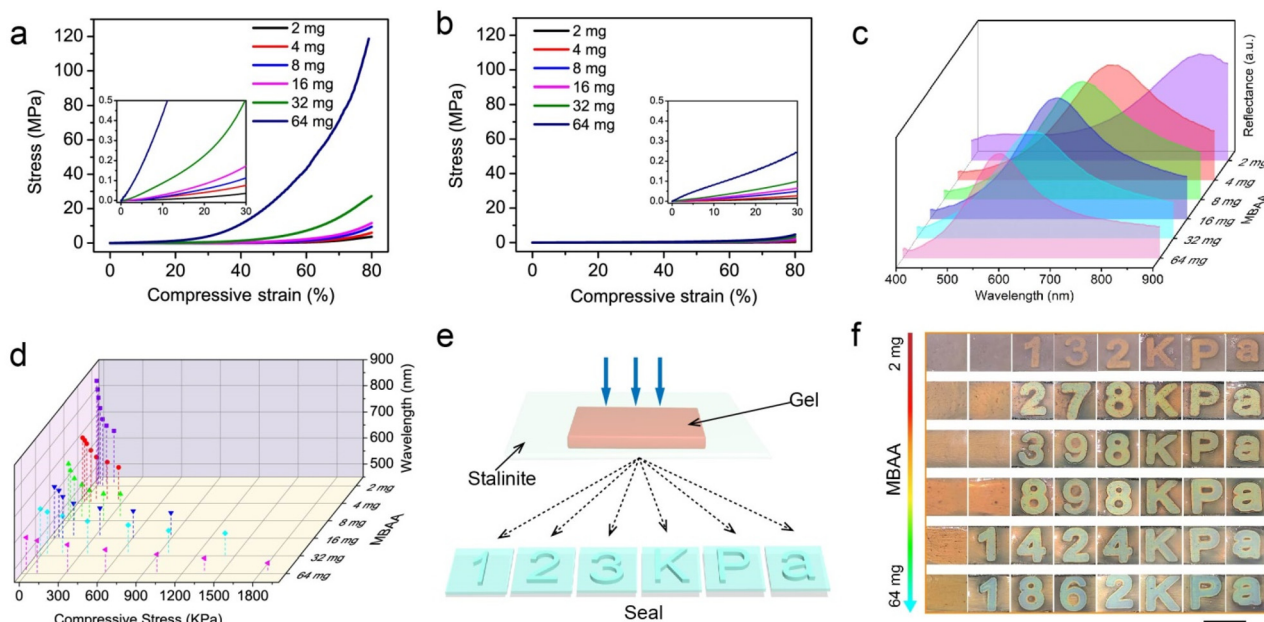

Fig. 5 Compressive stress−strain curves of (a) composite gels and (b) pure PDAAM-*co*-PAAM gel matrix prepared with different crosslinker contents; insets are partial enlarged views. (c) Reflection spectra of composite gels prepared with different crosslinker contents. (d) Phase diagram of reflection wavelength *versus* compressive stress. (e) Schematic diagram showing the structural color changes with compressive stress driven by the convex stamp. (f) Combined pattern photographs showing applied compressive stresses and structural color changes of composite gels prepared with different crosslinker contents.

thereby providing stable interfacial bridging and facilitating stress transfer from the soft polymer network to the hard nanoplates.[40–42]

Owing to its merits in adjustable high-strength mechanical behavior of the composite gels, we can achieve optical response to broad-range tunable stress by establishing the stress–strain-color correspondence. To this end, we first investigated the effect of crosslinker on the structural color. As displayed in Fig. 5c and S12,† the reflection wavelength of the samples is negatively correlated with the crosslinker content because the increased crosslinker leads to a decrease in the solvent content of the composite gels, thus resulting in a volume contraction. Subsequently, based on the quantitative relationships of compressive stress–strain and strain–spectra, we drew the phase diagrams of reflection wavelength *versus* compressive stress for the composite gels with different mechanical strengths, successfully realizing the optical response to different ranges of compressive stress, as shown in Fig. 5d and S15.† It can be seen that a stronger mechanical force is required to drive the reflecting wavelength blue-shift as the mechanical strength of the composite gels increases. Importantly, different compressive stresses can provide visual feedback through structural color changes. As a demonstration experiment, we prepared acrylic convex stamps with numbers ("0–9") and letters ("K, P, a"), and compressed a composite gel on the stamp using stalinite, as depicted in Fig. 5e. When a sample was compressed separately on different stamps, its structural color would blue-shift and clearly outlines the corresponding number/letter pattern. By combining these patterns, the applied compressive stress was artificially displayed (Fig. 5f). For example, with the increase in MBAA content in solution A, the maximum compressive stress that could be identified by virtue of the structural color change gradually increased from ∼132 KPa to ∼1862 KPa, indicating that broad-range compressive stress could be visualized *via* modulating the mechanical strength of the gels. It should be emphasized that the compressive stress values are estimated from the phase diagram in Fig. 5d. Moreover, when the compressive stress applied to the same sample is gradually increased, the structural color changes from red to green accordingly (Fig. S16†). These demonstrations show that composite gels have great application prospects in visualizing the direction of high stress indicators. These demonstrations show that composite gels have great application prospects in the field of visual high-stress indicators and displays.

Conclusions

In summary, we present a new type of composite gels with assembled layers of nanoplates featuring large strength, remarkable low working temperature, and excellent anti-drying performance. The composite gels are prepared by directionally fixing the photonic LC (nematic) of α-ZrP nanoplates in the soft PDAAM-*co*-PAAM matrix while undergoing replacement of Gly–water and subsequent heat treatment for dehydration. As

a result, the obtained alternating hard/soft composite architecture produces nacre-like structural colors with broad-spectrum wavelength derived from the interaction with natural light. This structural color can be fine-regulated from ∼780 nm to ∼445 nm by varying the concentration of α-ZrP nanoplates and Gly. At the same time, the composite gels retain optical stability (7 d) under the arid condition (35% RH) and demonstrate extreme anti-freezing behavior down to −80 °C. Therefore, the composite gels exhibit excellent dynamic reversible mechanochromic properties in ambient air. Furthermore, it has superior high mechanical strength based on the high fraction of hard α-ZrP nanoplates with a soft polymer to form dense hydrogen bonding. More importantly, the mechanical properties are modulated in a large window by changing the crosslinker concentration to control the crosslinking density and solvent content synergistically. For instance, the compressive strength can leap from ∼3.66 MPa to ∼119 MPa under 80% compression strain; the tensile fracture strength can increase from ∼0.23 MPa to ∼2.59 kPa simultaneously. By virtue of the widely adjustable high mechanical properties and strain-induced color changes, the composite gels can visually identify stresses in different ranges, such as from 0 KPa–132 KPa to 0 KPa–1862 KPa. We believe this work provides a general inspiration for the preparation of highly designable mechanical properties of structural-colored gels using the small aspect ratio nanoplates, which would broaden the practical applications of mechanochromic sensors in the fields of high-stress indicators and displays.

Author contributions

Yunpeng Wang: experimental investigation, data curation, formal analysis, project supervision, roles/writing – original draft, conceptualization. Xinyu Kan, Yaru Liu: investigation, validation. Jie Ju, Xi Yao: conceptualization, funding acquisition, resources, writing – review & editing.

Conflicts of interest

There are no conflicts to declare.

Acknowledgements

References

1 J. Teyssier, S. V. Saenko, D. van der Marel and M. C. Milinkovitch, *Nat. Commun.*, 2015, **6**, 6368.
2 L. Li, S. Kolle, J. C. Weaver, C. Ortiz, J. Aizenberg and M. Kolle, *Nat. Commun.*, 2015, **6**, 6322.

3 D. E. Morse and E. Taxon, *Appl. Phys. Lett.*, 2020, **117**, 220501.

4 Y. Wu, R. Sun, J. Ren, S. Zhang and S. Wu, *Adv. Funct. Mater.*, 2022, **33**, 2210047.

5 C. Duan, Z. Cheng, B. Wang, J. Zeng, J. Xu, J. Li, W. Gao and K. Chen, *Small*, 2021, **17**, 2007306.

6 P. Ganter and B. V. Lotsch, *Mol. Syst. Des. Eng.*, 2019, **4**, 566–579.

7 T. H. Park, S. Yu, J. Park and C. Park, *Sci. Technol. Adv. Mater.*, 2023, **24**, 2156256.

8 P. Shen, Y. Zhang, Z. Cai, R. Liu, X. Xu, R. Li, J.-J. Wang and D. A. Yang, *J. Mater. Chem. C*, 2021, **9**, 5840–5857.

9 Y. Zhang, Y. Wang, H. Wang, Y. Yu, Q. Zhong and Y. Zhao, *Small*, 2019, **15**, 1902198.

10 D. Y. Kim, S. Choi, H. Cho and J. Y. Sun, *Adv. Mater.*, 2019, **31**, 1804080.

11 J. Chen, L. Xu, M. Yang, X. Chen, X. Chen and W. Hong, *Chem. Mater.*, 2019, **31**, 8918–8926.

12 B. Kong, R. Liu, Y. Cheng, Y. Shang, D. Zhang, H. Gu, Y. Zhao and W. Xu, *Adv. Sci.*, 2022, **9**, 2203096.

13 Y. Wang, W. Niu, C. Y. Lo, Y. Zhao, X. He, G. Zhang, S. Wu, B. Ju and S. Zhang, *Adv. Funct. Mater.*, 2020, **30**, 2000356.

14 H. M. Zhang, Y. P. Wang, S. F. Zhang and W. B. Niu, *ACS Appl. Mater. Interfaces*, 2022, **14**, 54936–54945.

15 J. Wang, Q. Cheng, S. Feng, L. Zhang and C. Chang, *J. Mater. Chem. C*, 2021, **9**, 6344–6350.

16 Y. Wang, L. Shang, G. Chen, L. Sun, X. Zhang and Y. Zhao, *Sci. Adv.*, 2020, **6**, eaax8258.

17 Z. Zhang, Z. Chen, Y. Wang and Y. Zhao, *Proc. Natl. Acad. Sci. U. S. A.*, 2020, **117**, 18310–18316.

18 Y. Wang, X. Cao, J. Cheng, B. Yao, Y. Zhao, S. Wu, B. Ju, S. Zhang, X. He and W. Niu, *ACS Nano*, 2021, **15**, 3509–3521.

19 H. B. Yao, J. Ge, L. B. Mao, Y. X. Yan and S. H. Yu, *Adv. Mater.*, 2014, **26**, 163–187.

20 Z. Sun, T. Liao, W. Li, Y. Qiao and K. Ostrikov, *Adv. Funct. Mater.*, 2019, **29**, 1901460.

21 S. Hao, Q. Fu, L. Meng, F. Xu and J. Yang, *Nat. Commun.*, 2022, **13**, 6472.

22 Y. Yang, X. Li, M. Chu, H. Sun, J. Jin, K. Yu, Q. Wang, Q. Zhou and Y. Chen, *Sci. Adv.*, 2019, **5**, eaau9490.

23 H. L. Gao, S. M. Chen, L. B. Mao, Z. Q. Song, H. B. Yao, H. Colfen, X. S. Luo, F. Zhang, Z. Pan, Y. F. Meng, Y. Ni and S. H. Yu, *Nat. Commun.*, 2017, **8**, 287.

24 P. H. Michels-Brito, V. Dudko, D. Wagner, P. Markus, G. Papastavrou, L. Michels, J. Breu and J. O. Fossum, *Sci. Adv.*, 2022, **8**, eabl8147.

25 Y. T. Xu, U. V. Mody and M. J. MacLachlan, *Nanoscale*, 2021, **13**, 7558–7565.

26 K. El Rifaii, H. H. Wensink, C. Goldmann, L. Michot, J. P. Gabriel and P. Davidson, *Soft Matter*, 2021, **17**, 9280–9292.

27 E. Mouri, C. Ogami, T. Fukumoto and T. Nakato, *Chem. Lett.*, 2020, **49**, 717–720.

28 M. Wong, R. Ishige, T. Hoshino, S. Hawkins, P. Li, A. Takahara and H.-J. Sue, *Chem. Mater.*, 2014, **26**, 1528–1537.

29 K. Sano, Y. S. Kim, Y. Ishida, Y. Ebina, T. Sasaki, T. Hikima and T. Aida, *Nat. Commun.*, 2016, **7**, 12559.

30 N. Miyamoto and T. Nakato, *Isr. J. Chem.*, 2012, **52**, 881–894.

31 W. Q. Yang, S. Yamamoto, K. Sueyoshi, T. Inadomi, R. Kato and N. Miyamoto, *Angew. Chem., Int. Ed.*, 2021, **60**, 8466–8471.

32 M. Zeng, D. King, D. Huang, C. Do, L. Wang, M. Chen, S. Lei, P. Lin, Y. Chen and Z. Cheng, *Proc. Natl. Acad. Sci. U. S. A.*, 2019, **116**, 18322–18327.

33 M. Iwata, M. Teshima, T. Seki, S. Yoshioka and Y. Takeoka, *Adv. Mater.*, 2017, **29**, 1605050.

34 Q.-F. Guan, H.-B. Yang, C.-H. Yin, Z.-M. Han, K.-P. Yang, Z.-C. Ling and S.-H. Yu, *ACS Mater. Lett.*, 2021, **3**, 243–248.

35 Y. N. Ye, M. A. Haque, A. Inoue, Y. Katsuyama, T. Kurokawa and J. P. Gong, *ACS Macro Lett.*, 2021, **10**, 708–713.

36 J. Wu, Z. Wu, Y. Wei, H. Ding, W. Huang, X. Gui, W. Shi, Y. Shen, K. Tao and X. Xie, *ACS Appl. Mater. Interfaces*, 2020, **12**, 19069–19079.

37 Q. Yu, Z. Qin, F. Ji, S. Chen, S. Luo, M. Yao, X. Wu, W. Liu, X. Sun, H. Zhang, Y. Zhao, F. Yao and J. Li, *Chem. Eng. J.*, 2021, **404**, 126559.

38 F. Chen, D. Zhou, J. Wang, T. Li, X. Zhou, T. Gan, S. Handschuh-Wang and X. Zhou, *Angew. Chem., Int. Ed.*, 2018, **57**, 6568–6571.

39 X.-M. Xing, G.-M. Liu, Y.-W. Ding and G.-Z. Zhang, *Chin. J. Polym. Sci.*, 2014, **32**, 531–539.

40 Q. Chen, Z. Ma, Z. Wang, L. Liu, M. Zhu, W. Lei and P. Song, *Adv. Funct. Mater.*, 2021, **32**, 2110782.

41 L. Han, K. Liu, M. Wang, K. Wang, L. Fang, H. Chen, J. Zhou and X. Lu, *Adv. Funct. Mater.*, 2018, **28**, 1704195.

42 B. Wang and A. Walther, *ACS Nano*, 2015, **9**, 10637–10646.